Shock Competition and a Model for Circulation Deposition in Shock-Ellipse Interactions

Ravi Samtaney[1], Jaideep Ray[2], Norman J. Zabusky[2]

NAS-98-016

December 1998

Abstract

We identify two different modes of interaction for planar shocks accelerating heavy prolate gaseous ellipses. These modes arise from different interactions of the incident and transmitted shocks on the leeward side of the ellipse. The principal parameters governing the interaction are the Mach number of the shock (M), the ratio of the density of the ellipse to the ambient gas density, $(\eta, \eta > 1)$, γ_0, γ_b (the ratios of specific heats of the two gases), λ (the aspect ratio). A time ratio $t_T/t_I(M, \eta, \lambda, \gamma_0, \gamma_b)$, which characterizes the mode of interaction, is derived. The two modes yield different mechanisms of the baroclinic vorticity generation. We model the net baroclinic circulation generated on the interface by both the incident and transmitted shocks and validate the model via numerical simulations of the Euler equations. In the range $1.2 \leq M \leq 3.5$, $1.54 \leq \eta \leq 5.04$ and $\lambda = 1.5$ and 3.0, our model predicts the baroclinic circulation to within 10 % of the simulation results.

[1]MRJ Technology Solutions Inc., NASA Ames Research Center, Moffett Field, CA 94035-1000. email: samtaney@nas.nasa.gov

[2]Dept. of Mech. and Aero. Engg., Rutgers University, Piscataway NJ 08854-8058. email: nzabusky@vizlab.rutgers.edu, jaray@vizlab.rutgers.edu

1

1   Introduction

Recently, there has been an active interest in the field of shock interactions with density–stratified interfaces. Such studies [1] are motivated by a desire to understand turbulent mixing in SCRAMJETS, Inertial Confinement Fusion as well as astrophysical phenomena related to supernovae. Furthermore, the shock interactions with a density–stratified interface may be considered a canonical problem in compressible hydrodynamics [2].

In this paper, we focus on the interaction of a planar shock accelerating a prolate, heavy (i. e., heavier than ambient) gas ellipse. The physical picture is that of a shock (also called the incident shock) of Mach number M, propagating in an infinite gaseous medium of density ρ_0, pressure p_0, and ratio of specific heats γ_0, and striking a prolate heavy gas ellipse of aspect ratio λ and minor axis $2b$, density ρ_b, pressure p_b, and ratio of specific heats γ_b. In this investigation, we use adjective "prolate" (resp. "oblate") to qualify an ellipse whose minor (resp. major) axis is parallel to the normal to the incident shock front. The gases used in this investigation and their properties are shown in Table 1. Fig. 1 depicts a schematic of the setup. Due to symmetry, only the top half is shown.

The incident shock (IS), on striking the interface between the elliptical bubble and the ambient gas, refracts into a transmitted shock (TS) and a reflected wave. Two generic classes of interactions exist: one where the IS moves faster than the TS (fast-slow or f/s) and vice versa (slow-fast or s/f). For the parameters considered in this paper, f/s (s/f) interactions are observed when $\eta = \rho_b/\rho_0 > 1$ ($\eta < 1$). The reflected wave is usually a shock for a f/s interaction and a rarefaction for s/f. If the IS, TS and the reflected wave meet at a *node* on the interface, the refraction is called *regular*.

As the incident shock traverses the elliptical interface, it generates a layer of vorticity baroclinically. We identify two different modes of baroclinic generation of circulation. These mechanisms are associated with *shock competition* on the leeward side of the bubble. The circulation deposited is proportional to the strength of the two counter–rotating dipolar vortices which emerge from the interaction at late time (by which we mean time exceeding at least ten ellipse passage times by the incident shock). These have been observed in simulations and experiments of shock interactions with circular cylinders, and their evolution may be explained simply in terms of incompressible vortex dynamics. Thus our explicit goal is to derive a reduced model

to quantify the baroclinic circulation on the interface.

Investigations of shock–accelerated circular cylinders were done experimentally by Haas and Sturtevant ($M \leq 1.3$) [3] and Jacobs ($M \leq 1.15$) [4], and numerically by Quirk and Karni ($M = 1.22$, radius resolved by 450 grid cells) [5] and McKee et al. ($M = 10$, radius resolved by 240 grid cells) [6]. Three–dimensional numerical simulations of shock–ellipsoid interactions were done by Xu and Stone ($M = 10$, major axis resolved by 128 grid cells) [7]. The evolution of interfaces containing baroclinic vorticity has been studied and quantified by Hawley and Zabusky [8] and Yang et al. [9]. A starting point in the development of our model is the model for circulation deposition on heavy circular cylinders by Samtaney and Zabusky [10] and baroclinic circulation quantifications for s/f interfaces by Samtaney et al. [11].

2 Numerical Simulations

2.1 Governing Equations

We first present results from numerical simulations to demonstrate the shock–competition mentioned above. Since viscous effects are expected to be negligible during the vorticity deposition phase of the shock–ellipse interaction, we adopt an inviscid model for simulation purposes. We make the following assumptions: the flow is inviscid, the gases are perfect, and there are no chemical reactions between the two gases, which are further assumed to be in thermal equilibrium. The governing equations (the compressible Euler equations) in conservative form are

$$\mathbf{U}_t + \mathcal{F}(\mathbf{U})_x + \mathcal{G}(\mathbf{U})_y = 0, \tag{1}$$

where

$$
\begin{aligned}
\mathbf{U} &= \{\rho, \rho u, \rho v, E, \rho \zeta\}^T, \\
\mathcal{F}(\mathbf{U}) &= \{\rho u, \rho u^2 + p, \rho u v, (E+p)u, \rho \zeta u\}^T, \\
\mathcal{G}(\mathbf{U}) &= \{\rho v, \rho u v, \rho v^2 + p, (E+p)v, \rho \zeta v\}^T,
\end{aligned}
$$

and E is the total energy, related to the pressure p by $p = (\gamma - 1)(E - \frac{1}{2}\rho(u^2 + v^2))$.

4

In the above equations, the field quantity $\zeta(\mathbf{x}, t)$, defined as the volume fraction of the incident gas, is used to track of the interface between the incident and transmitted gases. $\zeta(\mathbf{x}, t) \in [0, 1]$ and the level set $\zeta(\mathbf{x}, t) = 0.5$ is chosen to define the interface.

2.2 Initial and Boundary Conditions

The boundary conditions are post-incident shock values at the left boundary and quiescent flow $(p_b, \rho_b, \mathbf{u} = 0)$ at the right boundary. Reflecting boundary conditions ($\mathbf{u} \cdot \mathbf{n} = 0$, where $\mathbf{n}$ is the unit normal to the plane of the boundary) were enforced on the horizontal axis (axis of symmetry) and outflow boundary conditions were enforced on the top boundary. The ellipse is centered at the origin of the coordinate system, and only the top half of the ellipse is simulated. The initial condition for ζ is given by $\zeta(\mathbf{x}, 0) = 1(0)$ in the incident (transmitted) gas. A shock moving in the positive x-direction is initialized using the Rankine-Hugoniot jump conditions. The shock was initialized at $X_0 = 10\Delta x$ left of the interface which is initially smeared over $2\Delta x$ to $3\Delta x$.

2.3 Numerical Details

Our numerical method is a second-order accurate Godunov scheme and includes interface tracking. A complete exposition of the numerical method can be found in our previous paper [11]. The Godunov method gave rise to transverse oscillations behind the transmitted shock at high Mach numbers ($M > 2.75$) and high stratifications ($\eta > 5$), and consequently a second–order Equilibrium Flux Method (EFM) [12] was used for them.

It should be noted that no explicit artificial viscosity was used in these numerical methods. However these numerical methods do suffer from an implicit numerical viscosity which causes a local mixing of the incident and transmitted gases. The ratio of specific heats in a computational cell containing a mixture of the gases is calculated as

$$\gamma = \frac{\gamma_0 \zeta R_0 + \gamma_b (1 - \zeta) R_b}{\zeta R_0 + (1 - \zeta) R_b}, \tag{2}$$

where R_0 and R_b are gas constants of the incident and transmitted gas, respectively.

5

A uniform mesh is used for all the simulations. The simulation codes were validated in our previous studies [11, 13]. In Fig. 2 we establish convergence with respect to grid refinement for interfacial circulation deposition (Γ_{num}, [11]) on an ellipse. We plot the circulation for the parameter set $M = 1.5, \eta = 3.0, \lambda = 1.5, \gamma_0 = 1.4, \gamma_b = 1.172$, normalized by Mc_0b, as a function of time. We observe convergence for the interfacial circulation when the major axis of the ellipse was resolved by 180, 360, and 720 grid points. For the runs in this paper, the major axis will be resolved by 360 grid cells except where noted.

2.4   Normalization

For simplicity, we assume $p_b = p_0 = \rho_0 = 1$ and $\rho_b = \eta$. All length scales are normalized by b (equivalent to specifying $b = 1$), velocities by c_0, the speed of sound in the ambient medium (equivalent to specifying $c_0 = 1$), and time by $t^* = b/c_0$, the half-bubble traversal time by a sound wave.

3   Shock–Competition

In this section, we first distinguish between two modes of interaction which arise on the leeward side of the ellipse. A time ratio is then derived which characterizes the mode of the interaction.

3.1   Classification

Here we describe the two modes on interaction. These modes are named a "Type I" and a "Type II" interaction. Fig. 3 shows a *Type I* interaction. The results are from an $M = 1.2, \eta = 5.04, \lambda = 1.5$ (Air-SF6) simulation. Density contours have been plotted over the normalized vorticity field (ω/ω_{max}, where $\omega_{max} = max(|\omega|)$) to juxtapose the shocks and the vorticity. The contour level $\zeta = 0.5$ denotes the center of the interfacial layer and is seen as the dark line in Fig. 3. Fig. 3(a) shows the transmitted shock (TS) approaching a local s/f interaction with the leeward side, while the incident shock (IS) has nearly completed its traversal. Fig. 3(b) shows an s/f interaction between TS and the *post–shocked* ambient gas on the leeward side of the ellipse in progress while the IS reflects off the horizontal axis, depositing opposite–signed vorticity. Thus the TS completes its traversal of the ellipse *after* the

IS. It is clear that there is circulation deposition first by the IS followed by circulation deposition by the TS. The windward edge of the ellipse shows a "staircase" effect due to discretization of the density interface. It plays no role in our discussion because it contains very little vorticity. Note that the incident shock compresses the ellipse, and therefore, the length of the minor axis is smaller than 2. Furthermore, the shock imparts a mean velocity to the ellipse along the x-axis. Due to this the ellipse does not appeared centered at the origin in Fig. 3.

Fig. 4 shows density contours, the mean interface location ($\zeta = 0.5$ contour), and the normalized vorticity field at three different times for a *Type II* interaction with $M = 2.75, \eta = 3.0$, and $\lambda = 3.0$ (Air-R22). The TS traverses the ellipse before the IS and interacts with it on the leeward side. There is circulation deposition by the IS which is prematurely terminated and a s/f deposition by the TS. In Fig 4(a) we see the incident shock (IS) traversing around the leeward side depositing negative vorticity, while the transmitted shock (TS) approaches the leeward interface. The nearly vertical "stalk" of the TS is about to undergo a local s/f interaction. In Fig. 4(b), we observe a complex shock system created by the TS-IS interaction. Vorticity generation on the interface by the IS is terminated, and the TS undergoes an s/f interaction with the *unshocked* ambient gas on the leeward side. In Fig. 4(c), TS has emerged from the bubble, and its interaction with the IS occurs *off* the interface. A slip line, formed as a result of the TS-IS interaction, is seen emanating from a triple point on TS. We also see the incipient rolling up of the interface, as discussed in [14]. Note that, as in the previous interaction, the ellipse gets compressed by the shock and translates along the x-axis.

From the above discussion, in essence we observe that the IS and the TS *compete* on the leeward side of the ellipse. It is precisely this shock–competition which determines the vorticity deposition mechanism.

Samtaney and Zabusky [10] identified three phases in the interaction of shocks with circular cylinders. We observe a variation of the same in shock–ellipse interactions. The traversal of the shock can be divided into the following phases :

- Phase (i) : In this phase, the shock undergoes regular refraction on the windward side of the ellipse. This phase ends when α, the local angle between the shock front and the ellipse, reaches a critical angle [10] at C in Fig. 5.

- Phase (ii) : This phase ends when the shock reaches the top of the ellipse (point B in Fig. 5), i. e., $\alpha = \pi/2$.

- Phase (iii) : This phase occurs on the leeward side of the ellipse (between B and D in Fig. 5). The incident shock traverses over the top and bends back to meet the interface almost at $\alpha = \pi/2$ [10]. However, if the incident shock is weak, it decomposes into a local region of compression waves near the interface. The effects of shock competition, as outlined above (secondary interactions involving TS and the premature termination of the IS traversal), are observed only in this phase of the interaction.

The different phases of the interaction are summarized in Fig. 5. A and D are the windward and leeward tips of the ellipse, respectively, while B is the top. Point C ($\equiv (-x_c, y_c)$) is the point where the shock refraction becomes irregular. C' is the mirror image on the leeward side. Phase(i) of the interaction occurs in $\widehat{AC}$, Phase(ii) in $\widehat{CB}$, and Phase(iii) in $\widehat{BC'D}$

3.2 Critical Time and Aspect Ratios

We now distinguish the shock–competition by means of the shock traversal time. To model these interactions, we make a few simplifying approximations.

1. We approximate the "stalk" of the TS as a plane shock of height y_c, $(-x_c, y_c)$ being the point on the interface where the incident shock refraction becomes irregular. In an irregular refraction at an elliptical interface, the TS system consists of a nearly vertical "stalk", topped by a triple point and a complex shock system. By approximating the TS as a plane shock of height y_c, we ignore the triple point and the complicated shock system associated with it.

2. We assume that the height and strength of the TS remain unchanged as it propagates through the inside of the ellipse.

3. On the leeward side of the ellipse, we adopt the near-normality ansatz [10], i. e., the IS is locally perpendicular to the interface.

8

We estimate the time taken by the IS to traverse the prolate elliptical interface by

$$
\begin{aligned}
t_I &= \frac{1}{M} \left[\int_A^B dx + \int_B^D dl \right] \\
&= \frac{1}{M} \left[1 + \lambda \mathcal{E} \left(\frac{\sqrt{\lambda^2 - 1}}{\lambda} \right) \right]
\end{aligned}
\tag{3}
$$

where dl is the infinitesimal arc length along the interface, and the points A, B and D have been defined in Fig. 5. Note that $\mathcal{E}(k)$ is a complete elliptic integral of the second kind. The time taken by the TS to traverse the interior of the ellipse is estimated by

$$
t_T = \frac{2}{M_T c_b},
\tag{4}
$$

where c_b is the speed of sound in the unshocked ellipse normalized by c_0, M_T is the Mach number of the transmitted shock. Note that M_T is calculated from a one dimensional f/s shock interaction (consult reference [10] for details). The ratio

$$
\frac{t_T}{t_I} = \frac{M}{M_T} \sqrt{\frac{\gamma_0}{\gamma_b}} \frac{2\sqrt{\eta}}{1 + \lambda \mathcal{E}(\sqrt{(\lambda^2 - 1)}/\lambda)},
\tag{5}
$$

determines the type of interaction. Since in a Type II interaction, the transmitted shock (TS) completes its traversal before the incident shock, it is characterized by $t_T/t_I < 1$. Type I interactions have $t_T/t_I > 1$. We also estimate the time taken by the TS to start an s/f interaction on the leeward side (alternatively, to terminate the primary circulation deposition by the IS) as

$$
t_c = \frac{1 + x_c}{M_T c_b}.
\tag{6}
$$

If γ_0 and γ_b are fixed, then the 3-tuple (ξ, η, λ) defines the parameter set for a given shock–ellipse interaction, where ξ is the normalized pressure ratio across the incident shock, given by

$$
\xi(M) = \frac{\frac{2\gamma}{\gamma+1}(M^2 - 1)}{1 + \frac{2\gamma}{\gamma+1}(M^2 - 1)},
$$

9

so that $\xi(M) \to 0(1)$ for weak (strong) shocks. Keeping (ξ, η) fixed, as λ is varied, for aspect ratios less than a critical aspect ratio ($\lambda < \lambda_c$), we observe a Type I interaction, while for $\lambda > \lambda_c$, we observe a Type II interaction. For $\lambda = \lambda_c$, we have $t_T/t_I = 1$. Note that Eq. 3 is valid only for prolate ($\lambda \geq 1$) ellipses. Since it is possible that $\lambda_c < 1$ for certain (ξ, η) combinations, Eq. 3 was reworked for oblate ellipses to give

$$t_I = \frac{1}{M}\left[1 + \mathcal{E}(\sqrt{1-\lambda^2})\right]. \tag{7}$$

t_T/t_I (Eq. 5) changes accordingly. In Fig. 6(a), we plot the surface $\lambda = \lambda_c(\xi, \eta)$ as a function of ξ and $1/\eta$ fixing the specfic heat ratios ($\gamma_0 = \gamma_b = 1.4$). The λ_c surface in (ξ, η, λ) space forms the boundary between Type I & II interactions. In Fig. 6(b) we show projected λ_c contours in the (ξ, η) space. We observe that in the (ξ, η) space there is a region where $\lambda_c < 1$. This implies that if only prolate ellipses are considered ($\lambda > 1$) then in this region one can only observe Type II interactions.

4 Quantification and Modeling of Baroclinic Circulation

Samtaney et al.([10], [11]) showed that the baroclinic circulation generation per unit length of a density–stratified interface (accurate to first order), normalized by c_0, is given by $\tilde{\sigma}_1 = \sigma_i(M, \eta, \gamma_0, \gamma_b)\sin\alpha$, where α is the local angle between the shock front and the interface and i denotes s/f or f/s. Equations for $\sigma_i(M, \eta, \gamma_0, \gamma_b)$, for both s/f and f/s interactions, are given in Appendix A for completeness. We assume (a) the incident shock strength M remains constant and (b) the incident shock is locally perpendicular to the interface on the leeward side of the bubble. Under these assumptions, in the absence of shock competition, the vorticity deposition on a heavy ellipse is given by

$$\begin{aligned} \Gamma_{f/s} &= \sigma_{f/s}(M, \eta, \gamma_0, \gamma_b)\left[\int_A^B \sin(\alpha)dl + \int_B^D \sin(\pi/2)dl\right] \\ &= \sigma_{f/s}(M, \eta, \gamma_0, \gamma_b)\left[1 + \lambda\mathcal{E}\left(\frac{\sqrt{\lambda^2-1}}{\lambda}\right)\right]. \end{aligned} \tag{8}$$

Points A, B, and D are defined in Fig. 5.

Type I interactions (characterized by $t_T/t_I > 1$) contain a primary f/s deposition by the IS and a secondary deposition by the TS. Thus

$$\begin{aligned} \Gamma_I &= \Gamma_{f/s} + \sigma_i(M_T, 1/\eta', \gamma_b, \gamma_0) \int_{C'}^{D} \sin(\alpha)dl \\ &= \Gamma_{f/s} + \sigma_i(M_T, 1/\eta', \gamma_b, \gamma_0)(1 - x_c), \end{aligned} \tag{9}$$

where $\eta' = \rho_b/\rho_0'$, ρ_0' is the *post-shocked* density of the ambient gas, approximated from a 1D shock–interface interaction. Subscript 'i' in equation 9 is either f/s or s/f depending upon η'.

It can be shown that in the absence of shock–competition (i. e., during the primary deposition), the time rate of baroclinic circulation deposition, up to first order, is a constant. Note that the circulation deposition in a Type II interaction contains two terms. The first term is due to the (prematurely terminated) deposition by the IS (approximated by $\Gamma_{f/s}t_c/t_I$), and the second term is the due to the s/f interaction of the TS at an interface of density ratio $1/\eta$. Therefore, the total circulation deposition in a Type II interaction is given by

$$\Gamma_{II} = \Gamma_{f/s}\frac{t_c}{t_I} + \sigma_{s/f}(M_T, 1/\eta, \gamma_b, \gamma_0)(1 - x_c). \tag{10}$$

We quantify the interfacial circulation from the numerical simulations (Γ_{num}, [10]) at the end of the TS traversal of the interior of the ellipse and plot Γ_{num}/Γ_I for $\eta = 3.0, \lambda = 1.5$ (Air-R22) and $\eta = 5.04, \lambda = 1.5$ (Air-SF6) simulations in Fig. 7. In Fig. 8 we plot Γ_{num}/Γ_I for $1.2 \leq M \leq 3.5$ for $\eta = 1.54, \lambda = 1.5$ (Air-CO2) and $\eta = 3.0, \lambda = 3.0$(Air-R22). The difference in cirulation deposition in numerical simulations, and the model is less than 10 % for both types of interactions.

5   Conclusion

In summary, shock–ellipse interactions are characterized by leeward–side shock competition. A time ratio (of the ellipse traversal times of the incident and transmitted shocks) governs the competition and is used to demarcate the two types of interactions observed. For a given shock strength and gas pair, there exists a critical aspect ratio of the elliptical cylinder for which the time ratio is unity. We show that for a certain region of the parameter

space, prolate ellipses can experience only one type of interaction. A simple model for the baroclinic circulation deposition during the interaction (which incorporates the effect of shock competition) has been proposed which agrees with results from numerical simulations to within 10 %.

Acknowledgements

A   Calculation of the circulation model terms

In this appendix, we provide, without details, sufficient information to calculate the terms ($\sigma_{s/f}$ and $\sigma_{f/s}$) in the model derived in section IV.

The baroclinic circulation generation per unit length of a fast–slow interface can be expressed as a series in $\sin\alpha$, where α is the local angle between the shock front and the interface. The coefficient of the first order term is $\sigma_{f/s}(M, \eta, \gamma_0, \gamma_b)$, and is given by[10]

$$\sigma_{f/s} = \frac{\gamma_0^{\frac{1}{2}}}{M}\left(\frac{1}{\gamma_b - 1}\frac{1 - \psi(p_{20}, \mu_b)}{\eta\gamma_0/\gamma_b} - \frac{1}{\gamma_0 - 1}\left(1 - \psi(p_{20}/p_1, \mu_0)\psi(p_1, \mu_0)\right)\right). \tag{11}$$

In the above equation p_1 is the pressure behind the incident shock (of Mach number M) and is given by

$$p_1 = 1 + \frac{2\gamma_0}{\gamma_0 + 1}(M^2 - 1). \tag{12}$$

Furthermore, p_{20} is the pressure behind the reflected shock for $\alpha \to 0$ and may be calculated by solving the following nonlinear algebraic equation,

$$\frac{p_1 - 1}{(\mu_0^2 + p_1)^{\frac{1}{2}}} - \frac{p_{20}/p_1 - 1}{(\mu_0^2 + p_{20}/p_1)^{\frac{1}{2}}}\psi^{\frac{1}{2}}(p_1, \mu_0) - \eta^{-\frac{1}{2}}\frac{p_{20} - 1}{(\mu_b^2 + p_{20})^{\frac{1}{2}}}\left(\frac{\gamma_0 + 1}{\gamma_b + 1}\right)^{\frac{1}{2}} = 0. \tag{13}$$

The function $\psi(\xi, \mu) \equiv \xi \frac{1 + \mu^2 \xi}{\mu^2 + \xi}$, and $\mu_i^2 = \frac{\gamma_i - 1}{\gamma_i + 1}$.

Likewise, for a slow-fast interface, one may express the baroclinic circulation generation as a series in $\sin \alpha$. The coefficient of the first term in the series is $\sigma_{s/f}(M, \eta, \gamma_0, \gamma_b)$ and is given by [11]

$$\sigma_{s/f} = \frac{1}{\gamma_0^{\frac{1}{2}} M} \left(\frac{\gamma_b}{\gamma_b - 1} \frac{1 - \psi(p_{20}, \mu_b)}{\eta} - \frac{\gamma_0}{\gamma_0 - 1} \left(1 - \left(\frac{p_{20}}{p_1} \right)^{\frac{\gamma_0 - 1}{\gamma_0}} \psi(p_1, \mu_0) \right) \right).$$
(14)

In the above equation, p_{20} is the pressure behind the transmitted shock for $\alpha \to 0$ and is calculated by solving the following nonlinear algebraic equation

$$\frac{(1 + \mu_0^2)^{\frac{1}{2}}}{\gamma_0} \frac{p_1 - 1}{(\mu_0^2 + p_1)^{\frac{1}{2}}} + \frac{2}{\gamma_0 - 1} \psi^{\frac{1}{2}}(p_1, \mu_0) \left(1 - \left(\frac{p_{20}}{p_1} \right)^{\frac{\gamma_0 - 1}{2\gamma_0}} \right) =$$

$$\frac{(1 + \mu_b^2)^{\frac{1}{2}}}{\gamma_b (\eta \gamma_0 / \gamma_b)^{\frac{1}{2}}} \frac{p_{20} - 1}{(\mu_b^2 + p_{20})^{\frac{1}{2}}}.$$
(15)

References

[1] *Proceedings of the Sixth International Workshop on the Physics of Compressible Turbulent Mixing*, 1998. Ed. G. Jourdan and L. Houas. Held at Marseilles, France, 18–21 June, 1997. Imprimerie Caractere, 26, Rue Saint Bruno, 13004 Marseilles, France.

[2] N. J. Zabusky. Vortex paradigm for accelerated inhomogeneous flows: Visiometrics for the Rayleigh–Taylor and Richtmyer–Meshkov environments. *Annual Reviews of Fluid Dynamics*, 31, To appear in 1999.

[3] J.F. Haas and B. Sturtevant. Interaction of weak shock waves with cylindrical and spherical gas inhomogeneities. *J.Fluid Mech.*, 181:41–76, 1987.

[4] J. W. Jacobs. Shock induced mixing of a light-gas cylinder. *J. Fluid Mech.*, 234:629–649, 1992.

[5] J. J. Quirk and S. Karni. On the dynamics of a shock-bubble interaction. *J. Fluid Mech.*, 318:129–163, 1996.

[6] C. F. McKee, R. Klein and P. Colella. On the hydrodynamic interaction of shock waves with interstellar clouds I. Nonradiative shocks in small clouds. *The Astrophysical Journal*, 420:213–236, 1994.

[7] J. Xu and J. M. Stone. The hydrodynamics of shock-cloud interactions in three dimensions. *The Astrophysical Journal*, 454:172–181, 1995.

[8] J.F. Hawley and N.J. Zabusky. Vortex paradigm for shock-accelerated density-stratified interfaces. *Phys. Rev. Lett.*, 63:1241–1244, 1989.

[9] X. Yang, I-L. Chern, N. J. Zabusky, R. Samtaney, and J. F. Hawley. Vorticity generation and evolution in shock-accelerated density-stratified interfaces. *Phys. Fluids A.*, 4:1531–1540, 1992.

[10] R. Samtaney and N.J. Zabusky. Circulation deposition on shock-accelerated planar and curved density stratified interfaces: Models and scaling laws. *J. Fluid Mech.*, 269:45–85, 1994.

[11] R. Samtaney, J. Ray, and Norman J. Zabusky. Baroclinic circulation generation on shock accelerated slow/fast gas interfaces. *Phys. Fluids*, 10(5):1217–1230, 1998.

[12] D. I. Pullin. Direct simulation methods for compressible ideal gas flow. *J. Comp. Phys.*, 34:231–244, 1980.

[13] R. Samtaney and D. I. Meiron. Hypervelocity Richtmyer–Meshkov instability. *Phys. Fluids*, 9:1783–1803, 1997.

[14] R. Samtaney and D. I. Pullin. On initial-value and self-similar solutions of the compressible Euler equations. *Phys. Fluids*, 8:2650–2655, 1996.

Table 1: Gas pairs.

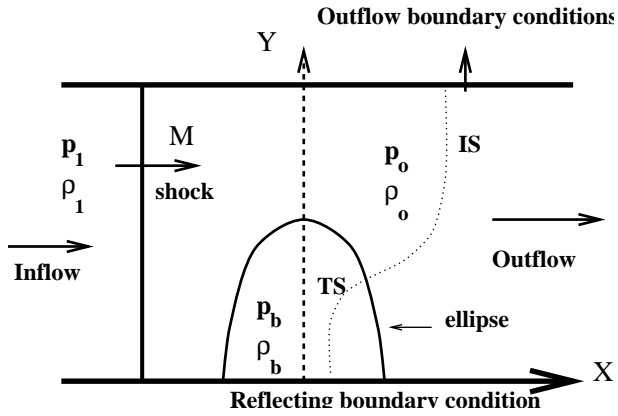| Gas	Gas Pairs		
Property	Air-CO2	Air-R22	Air-SF6
η	1.54	3.00	5.04
γ_0, γ_b	1.4, 1.297	1.4, 1.172	1.4, 1.0935

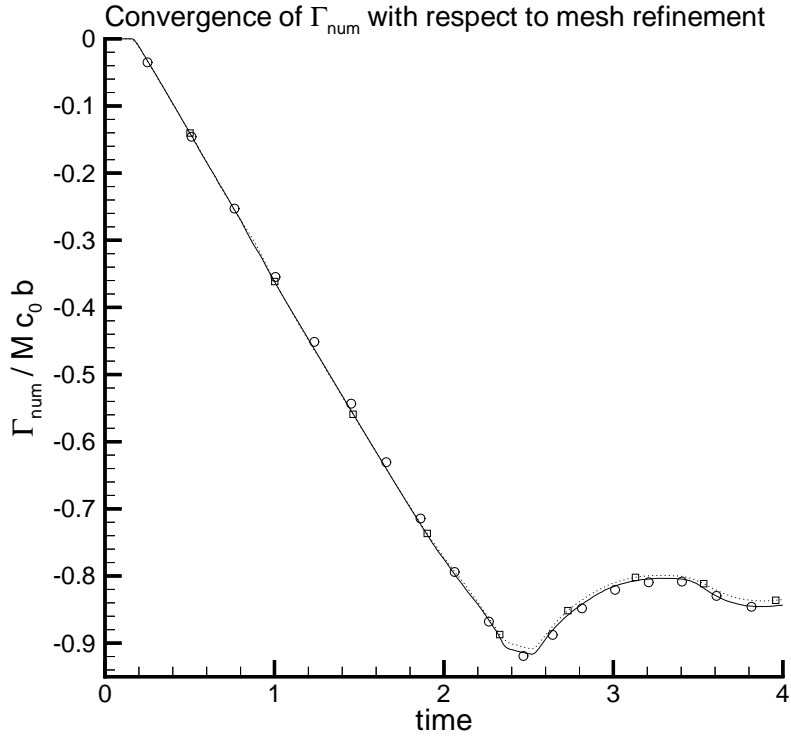Figure 1: Schematic of the physical setup. Due to symmetry, only the top half is shown.

Figure 2: Convergence study of baroclinic circulation (Γ_{num}) deposition on the ellipse by the shock. The circulation, normalized by Mc_0b, is plotted as a function of time. The parameters of the run are $M = 1.5, \eta = 3.0, \lambda = 1.5, \gamma_0 = 1.4, \gamma_b = 1.172$. The major axis of the ellipse was resolved by 180 (dotted line with □), 360 (solid line) and 720 (○) grid points.
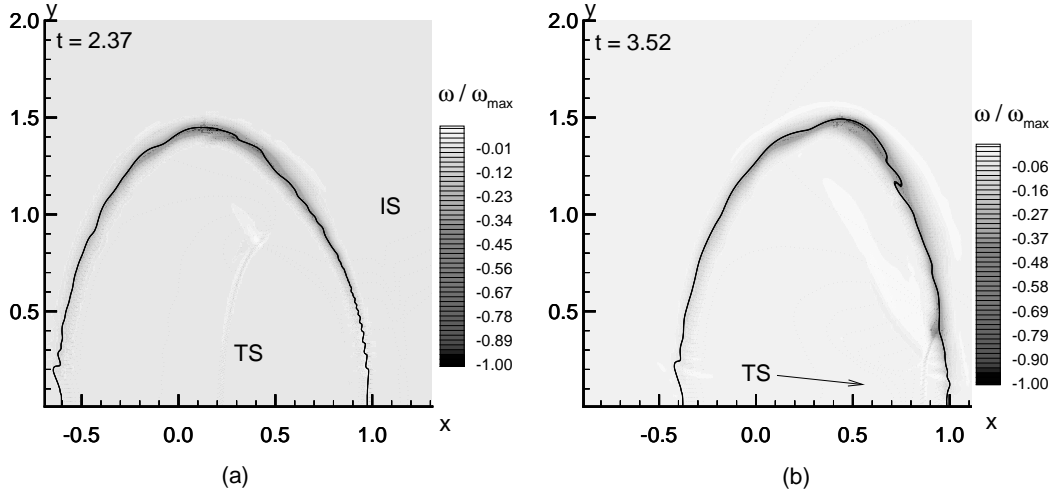
Figure 3: A Type I interaction at an Air-SF6 interface ($M = 1.2, \lambda = 1.5$). 16 density (ρ) contours (equally spaced between 1.8 and 12.1) have been overlaid on a normalized vorticity (ω/ω_{max} where $\omega_{max} = max(|\omega|)$) field. The interface $\zeta = 0.5$ is plotted using a solid line. In (a) we see the transmitted shock (TS) just before it undergoes a local s/f interaction with the leeward side of the interface while the incident shock traverses it. In (b) we see that the IS has reflected off the horizontal axis while TS undergoes a local s/f interaction with the leeward side of the ellipse. The density profile shows the strength of the shock after diffraction. $\omega_{max}b/Mc_0 = 8.62$, circulation deposition (numerical) at the end of the TS traversal: $\Gamma_{num}/Mc_0b = 0.863$. The simulation domain was $[-4.27 : 4.27] \times [0 : 2667]$.
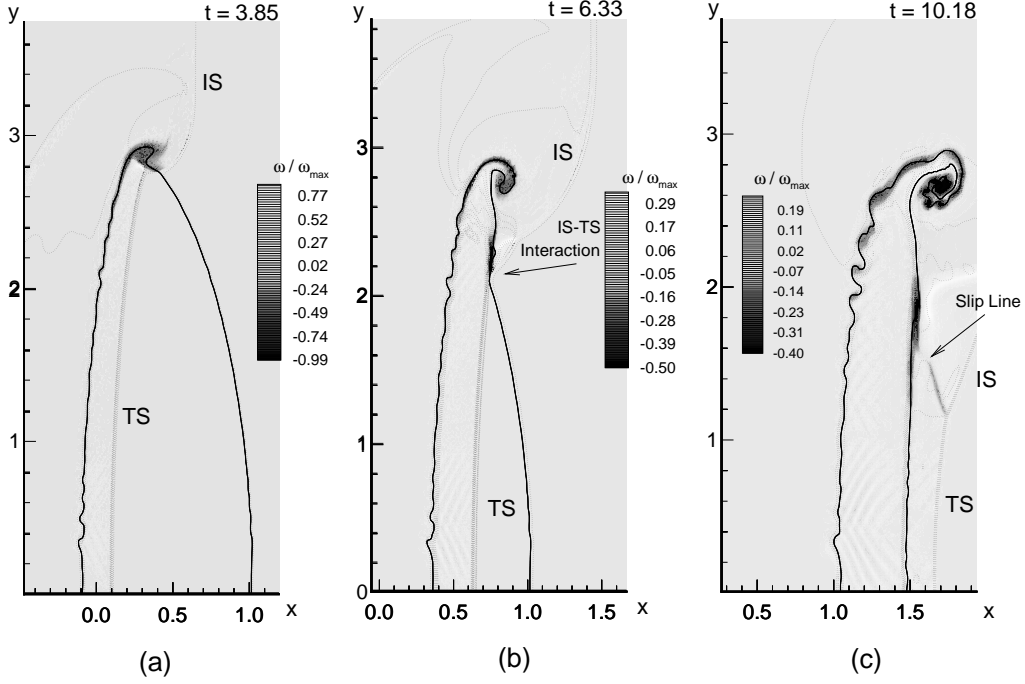
Figure 4: A Type II interaction at an Air-R22 interface ($M = 2.75, \lambda = 3.0$). 9 density (ρ) contours (equally spaced between 3 and 19) have been overlaid on a normalized vorticity (ω/ω_{max} where $\omega_{max} = max(|\omega|)$) field. The interface $\zeta = 0.5$ is plotted using a solid line. In (a) we see the transmitted shock (TS) just before it interacts with the incident shock (IS). In (b) the interaction is under way. In (c) we see that the transmitted shock has traversed through the ellipse before the incident shock. We also see a slip line emanating from a triple point on the TS, formed as a result of the TS-IS interaction on the leeward side. $\omega_{max}b/Mc_0 = 24.19$, circulation deposition (numerical) at the end of the TS traversal: $\Gamma_{num}/Mc_0b = 1.12$. For this simulation, the major axis was resolved by 720 grid points, the simulation domain was $[-2.133 : 2.133] \times [0 : 5.333]$.
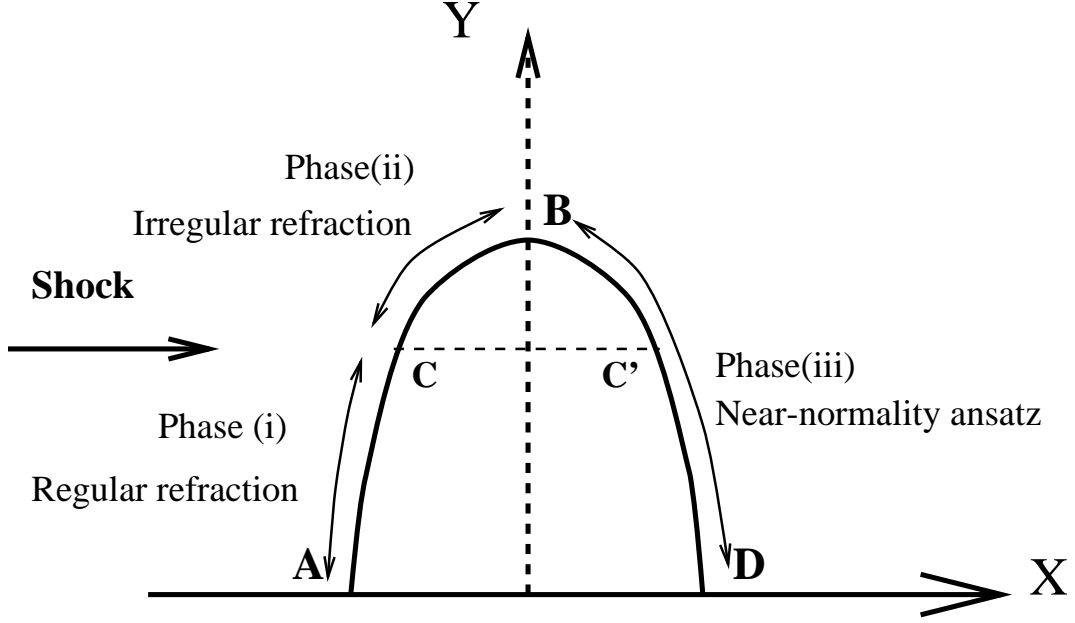
18

Figure 5: The different phases in a shock–ellipse interaction. A and D are the windward and leeward tips of the ellipse, respectively, while B is the top. Point C ($\equiv (-x_c, y_c)$) is the point where the shock refraction becomes irregular. C' is the mirror image on the leeward side. Phase(i) of the interaction occurs in $\widehat{AC}$, Phase(ii) in $\widehat{CB}$, and Phase(iii) in $\widehat{BC'D}$. Phase(i) is characterized by regular shock refraction and Phase(ii) by irregular refraction. The near-normality ansatz is employed in Phase(iii). Shock competition takes place in the section of the ellipse between C' and D.
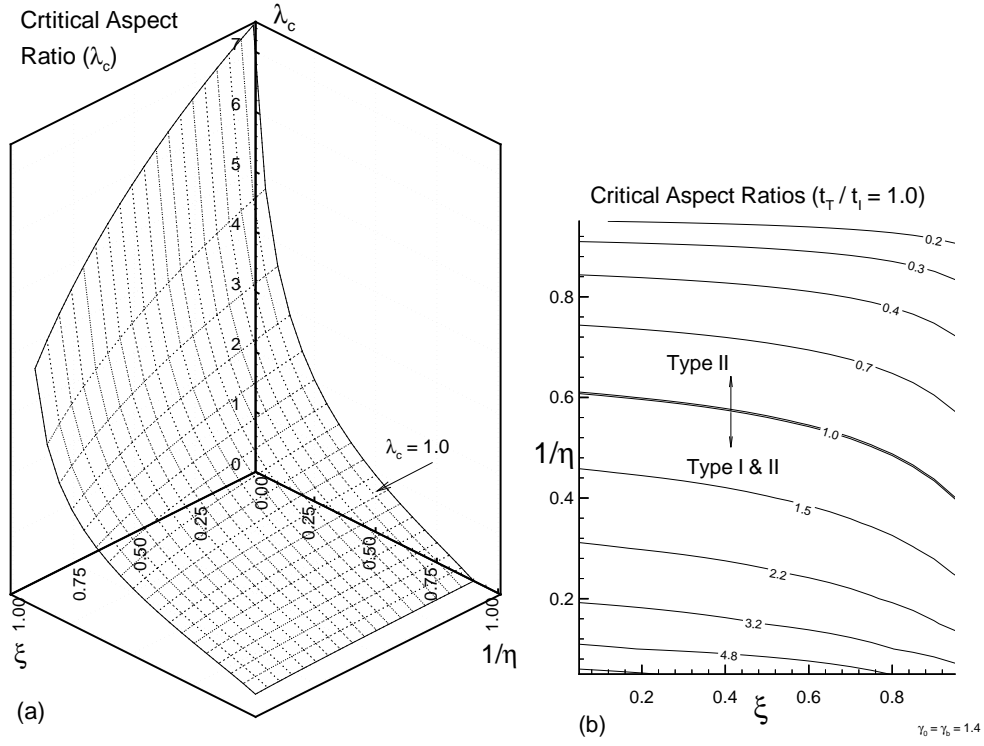
Figure 6: Critical aspect ratio (λ_c, Eq. 5 with $t_T/t_I = 1$) as a function of $1/\eta$ and ξ, the normalized pressure gradient across the incident shock. $\gamma_0 = \gamma_b = 1.4$. In (a) we plot the surface $\lambda = \lambda_c(\xi, \eta)$ to demarcate between Type I and Type II interaction spaces. For a Type I interaction $\lambda < \lambda_c(\xi, \eta)$ (below the surface) and for a Type II interaction $\lambda > \lambda_c(\xi, \eta)$ (above the surface). In (b) we project the λ_c surface to 2D. 10 exponentially spaced contours between 0.2 and 4.8 have been plotted. The arrows indicate the type of interactions experienced by *prolate* ellipses on either side of the $\lambda_c = 1.0$ contour.
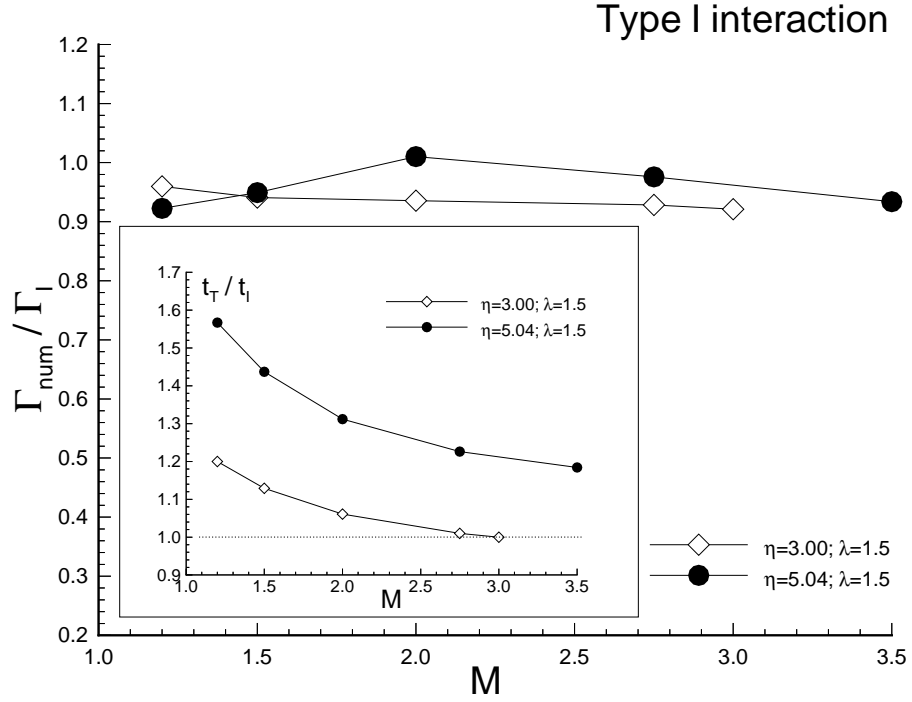
Figure 7: Γ_{num}/Γ_I (Eq. 9) for $1.2 \leq M \leq 3.5$ for Type I interactions. Results have been plotted for $\eta = 3.0, \lambda = 1.5$ (Air-R22, $\diamond$) and $\eta = 5.04, \lambda = 1.5$ (Air-SF6, $\bullet$). M is limited to 3.0 in the Air-R22 case since for $M > 3.0$, for a $\lambda = 1.5$ ellipse, the interaction becomes Type II. Inset: t_T/t_I has been plotted for all the cases to show the type of interaction.
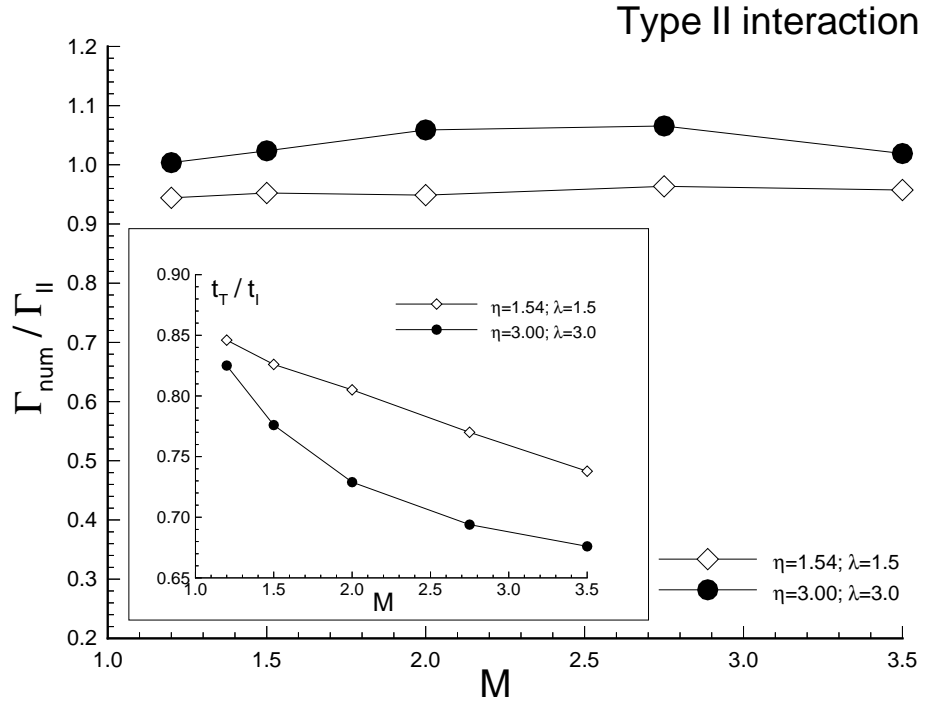
Figure 8: Γ_{num}/Γ_{II} (Eq. 10) for $1.2 \leq M \leq 3.5$ for Type II interactions. Results have been plotted for $\eta = 1.54, \lambda = 1.5$ (Air-CO2, $\bullet$) and $\eta = 3.0, \lambda = 3.0$ (Air-R22, $\diamond$). Inset: t_T/t_I has been plotted for all the cases to show the type of interaction.